Deliverable D 3.7
D3.7 Model of the laboratory pilot

Document type	**Deliverable D 3.7**
Document Version / Status	**1.6**
Primary Authors	**Alain GASSER, alain.gasser@univ-orleans.fr, UORL**
Distribution Level	**PU (Public)**
Project Acronym	**ATHOR**
Project Title	**Advanced THermomechanical multiscale mOdelling of Refractory linings**
Grant Agreement Number	**764987**
Project Website	**www.etn-athor.eu**
Project Coordinator	**Marc Huger, marc.huger@unilim.fr, UNILIM**
Document Contributors	**Alain GASSER, alain.gasser@univ-orleans.fr, UORL** **Mahmoud ALI, mahmoud.ali@univ-orleans.fr, UORL** **Thais SOARES, thais.soares@civil.uminho.pt, UMINHO** **Pratik GAJJAR, pratik.gajjar@civil.uminho.pt, UMINHO** **João PEREIRA, jpereira@civil.uminho.pt, UMINHO**

History of Changes

Version	Date	Author (Organization)	Change	Page
1.0	02.03.2022	Alain GASSER (UORL)	Summary	
1.1	27/03/2022	Mahmoud ALI (UORL)	Macro modelling approach	All
1.2	28.03.2022	Pratik GAJJAR (UMINHO)	Description, micro-modelling, and conclusion	All
1.3	29.03.2022	Pratik GAJJAR (UMINHO)	Corrections	All
1.4	31.03.2022	Glyn DERRICK (UNILIM) Marc HUGER (UNILIM)	Final check	All
1.5	15.04.2022	Pratik GAJJAR (UMINHO)	Corrections	All
1.6	17.05.2022	João PEREIRA (UMINHO) Alain GASSER (UORL)	Final modifications	All

European Commission | Horizon 2020 European Union funding for Research & Innovation

TABLE OF CONTENTS

1 INTRODUCTION 2
2 DESCRIPTION OF THE LABORATORY PILOT 3
2.1 Geometry 3
2.2 Material properties 4
2.3 Thermal load and boundary conditions 5
3 MICRO-MODELLING APPROACH 6
3.1 Thermal behaviour 7
3.2 Mechanical behaviour 8
4 MACRO-MODELLING APPROACH 10
5 CONCLUSION 14
6 REFERENCES 14

1 Introduction

Using the models of masonries developed in Task 3.4, the tests performed on the laboratory pilot (Task 4.4) are modelled numerically with finite element software. The comparison with the experimental results should allow the validation of the different masonry models. This report will review these various aspects.

Refractory materials exhibit complex behaviour. At lower temperatures their behaviour is brittle, while at high temperatures it becomes ductile [1]. The importance of creep for refractories in industrial applications has been shown in previous research [2][3]. These materials are used in large installations, which adds more complexity such as joint behaviour [4][5]. Therefore, developing a coherent modelling approach requires large-scale experimentation. Such tests are rarely performed due to the high cost involved and, when successful, they have been mainly done on masonry walls [6][7][8].

With the objective of gathering data for the validation of advanced numerical models, experimental characterisation of the refractory masonry that undergoes similar thermomechanical loadings as an industrial ladle was deemed necessary. Within ATHOR, an experimental installation was envisaged - a 3D pilot ladle. This represents a novel approach towards designing an experimental setup for large-scale refractory masonry. It requires an original test configuration, including designing the geometry, insulation, heating requirement, measurement devices and installation.

This 3D pilot model is a scaled representation of a ladle (Figure 1), which includes all the linings that would be present in an industrial ladle. It is expected to be tested under the thermal loads of similar magnitude to an industrial ladle without the presence of molten steel. This will also allow the characterisation and monitoring of the inner surface of the linings mechanically. The construction and testing of this experimental device will take place at the Ceramics Research Centre (CRC) of Tata Steel in IJmuiden, The Netherlands.

This document presents the predictive behaviour of the pilot ladle by considering different numerical approaches developed within the ATHOR project, namely, the micro-modelling method used by UMINHO and the macro-modelling approach developed by UORL. A detailed description of these approaches is presented in Deliverable D3.6 - Model of the nonlinear behaviour of masonry at high temperatures. These predictive numerical simulations will assist in the characterisation of the expected observed behaviour of the pilot ladle. In addition to the experimental result, these numerical results will aid in the calibration and validation of these different modelling approaches for large-scale industrial structures.

European Commission | Horizon 2020 European Union funding for Research & Innovation

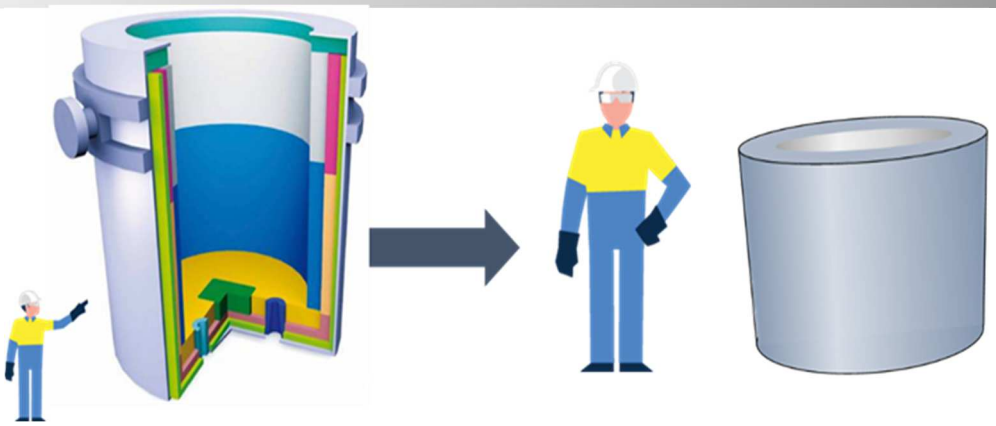

Figure 1 - Graphical representation of the laboratory scaled steel ladle

2 Description of the laboratory pilot

This section presents the description of the pilot steel ladle in terms of geometry, materials, thermal loads, and boundary conditions. A detailed description of the pilot ladle and measurement devices are presented in Deliverable 4.4. The final configuration of the pilot steel ladle is illustrated in Figure 2a. The current status of the pilot ladle, lined with insulation bricks and insulation board, is presented in Figure 2b. The pilot ladle will be rested on the ground and insulated by two insulation brick layers. The heating elements will be placed vertically and are supported by the top lid, which can be easily lifted. These experiments will be carried out at the Ceramics Research Centre of TATA Steel at IJmuiden, Netherlands.

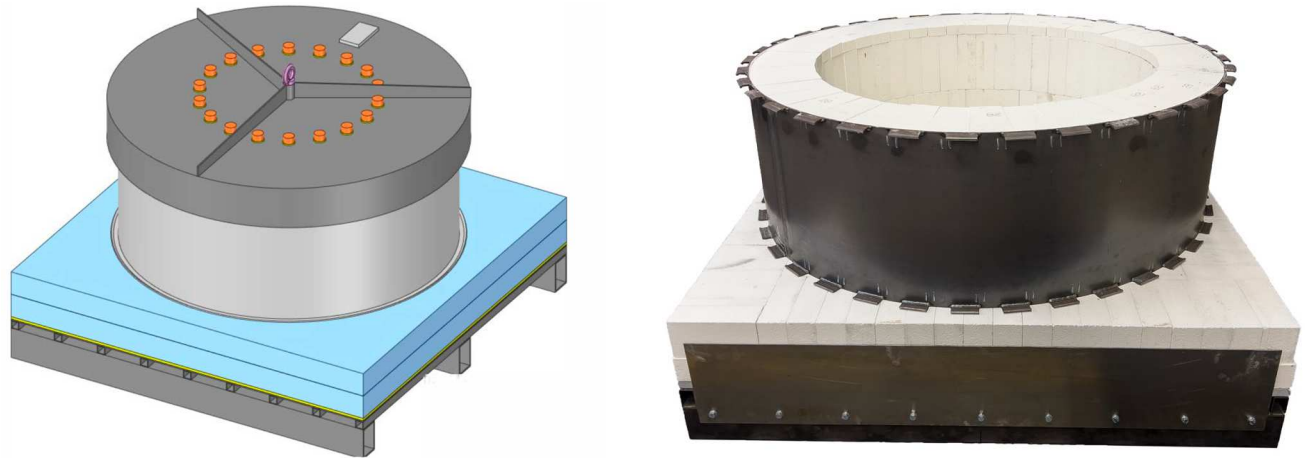

(a) (b)

Figure 2 - Laboratory scaled pilot steel ladle: a) Graphical representation of the whole assembly for the experiments on pilot steel ladle; b) Pilot steel ladle rested with insulation bricks on the ground support frame. The pilot ladle is lined with insulation boards (5 mm thickness) and insulation bricks.

2.1 Geometry

The dimensions of the 3D pilot ladle are 1500 mm in diameter and 500 mm in height (5 layers of bricks in wear linings). Figure 3 presents the global overview of the 3D pilot ladle. Different refractory linings are also shown, identical in thickness to an industrial steel ladle. Due to the change in geometry, the bricks in the wear lining will need to be cut. The modified dimensions of the brick and the number of bricks required is also shown in the figure. The shape of the safety and insulating linings do not need to be altered.

European Commission | Horizon 2020 European Union funding for Research & Innovation

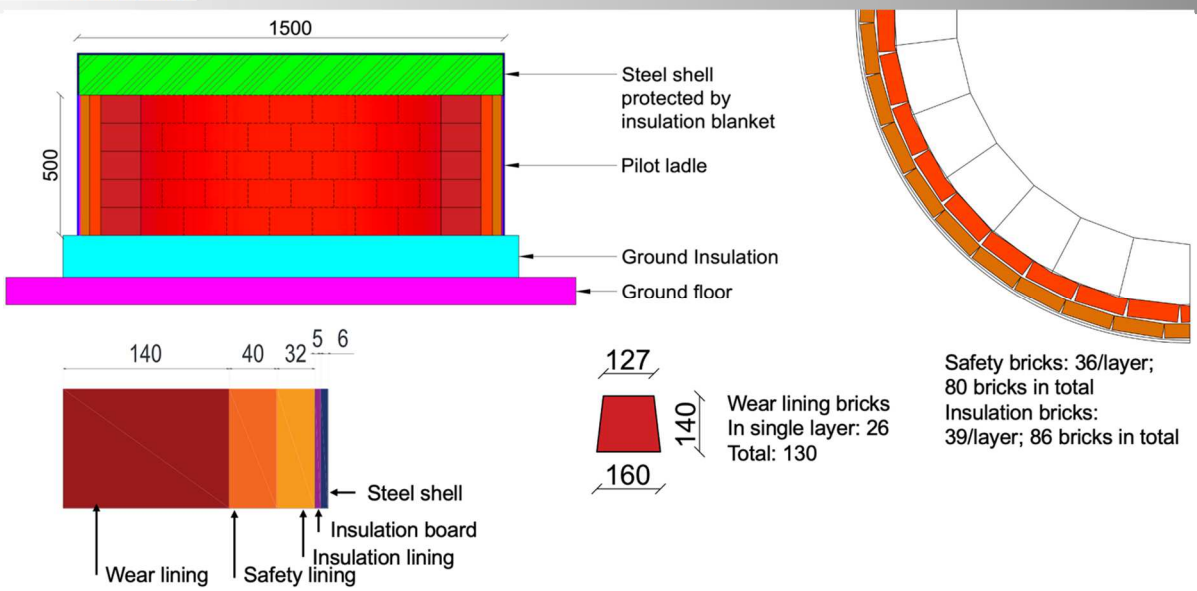

Figure 3 - Graphical illustration of the 3D pilot steel ladle showing the global view, configuration and thickness of the refractory linings and numbers of bricks required for the construction.

2.2 Material properties

Many refractory materials are available on the market depending on the location and purpose (i.e. mechanical resistance, chemical performance and thermal insulation) of the refractory materials in the different layers of the lining. Thus, different steel producers can select specific refractory materials. The refractory materials expected to be used in the pilot steel ladle are the same as those used in the industrial steel ladle at Tata Steel, as presented in Table 1. The working lining of the pilot is without mortar, and the subsequent permanent lining is composed of refractory bricks and mortars.

Table 1 - Materials used in the pilot steel ladle linings.

Lining	Material
Working Lining	Fired Alumina Spinel Bricks
Permanent Lining	Bauxite Bricks Chromite Bricks Insulation Board
Mortars	Fire setting mortar Air hardening mortar
Steel Shell	Steel

The thermomechanical properties of the Alumina Spinel bricks used in the working linings are evaluated in detail within the ATHOR project [9]-[11]. Material properties used in the numerical simulation is shown in Table 2. Moreover, a detailed description of these properties can be found in Deliverable 3.6. Temperature-dependent thermomechanical properties of other materials are shown in Table 3. In the table, ρ, k, C_p, E, and CTE refers to the density, thermal conductivity, specific heat, Young's modulus and coefficient of thermal expansion of the material, respectively. The permanent lining consists of two different types of refractory materials. For simplicity in the numerical modelling, an equivalent isotropic behaviour (the behaviour of the brick) of the permanent lining is assumed.

Table 2 - Alumina spinel bricks material properties used in thermomechanical simulation.

Properties		Value						
Physical	***Temperature (°C)***	20	200	400	800	1000	1200	1400
	E (GPa)	7.0	-	-	6.0	4.9	3.6	1.5
	Poisson's ratio (-)	0.2						
	ρ (kg/m3)	3130						
Thermal	***Temperature (°C)***	25	200	400	800	1000	1200	1500
	k (W/mK)	6.42	4.85	3.79	2.94	2.66	2.41	
	Cp (J/kgK)	805	1073	1161	1263	1293	1318	
	CTE (10-6K-1)	5.40	7.08	7.56	8.23	8.47	8.66	8.65

European Commission | Horizon 2020 European Union funding for Research & Innovation

Table 3 - Thermomechanical properties of the materials used in the different layers of the pilot steel ladle.

Lining	Properties	
Permanent Lining	ρ (kg/m^3)	2660
	k (W/mK)	2.6 at 400 °C 2.1 at 800 °C 2.0 at 1200 °C
	C_p (J/kgK)	890 at 200 °C 1144 at 1200 °C
	E (GPa)	4.5 at 800 °C 3.5 at 1000 °C 1.0 at 1200 °C
	CTE ($10^{-6}K^{-1}$)	6
Insulation board	ρ (kg/m^3)	510
	k (W/mK)	0.15 at 250 °C 0.25 at 800 °C 0.34 at 1350 °C
	C_p (J/kgK)	1047
	E (GPa)	0.3
	CTE ($10^{-6}K^{-1}$)	9
Steel Shell	ρ (kg/m^3)	7840
	k (W/mK)	47.3 at 200 °C 42.3 at 350 °C 37.3 at 500 °C
	C_p (J/kgK)	530 at 200 °C 666 at 500 °C
	E (GPa)	210 at 20 °C 170 at 400 °C
	CTE ($10^{-6}K^{-1}$)	12

2.3 Thermal load and boundary conditions

During the experiment, the thermal load will be applied with eighteen silicon carbide heating elements placed 138 mm from the surface of the working lining. The thermal load will be applied at a rate of 2 °C/min to increase furnace temperature from ambient temperature to 1550 °C in 12.75 hours. Once the desired temperature is achieved, it will hold the same furnace temperature of 1550 °C for additional 12 hours, as shown in Figure 4.

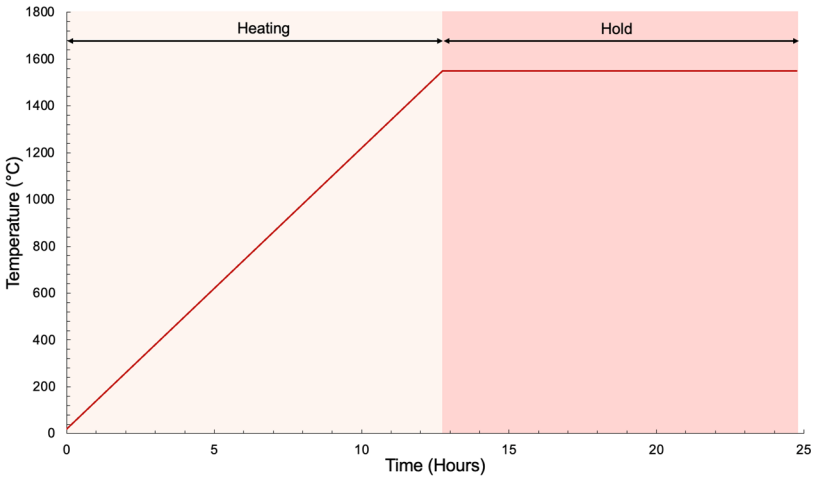

Figure 4 - Application of thermal load in furnace showing heating and holding period.

European Commission | Horizon 2020 European Union funding for Research & Innovation

In the absence of the experimental data, the following thermal loading conditions are considered for the numerical simulations presented in this document (These conditions were derived from the thermal measurement data presented for an industrial steel ladle in *Deliverable D4.5: In-situ measurements on industrial steel ladle finished*).

- The initial temperature of 20 °C is applied to the whole assembly.
- The steel shell is exposed to a constant temperature of 20 °C with a heat transfer coefficient α of 10 W/m^2/K.
- Heating in 12.75 hours to 1550 °C with a heat transfer coefficient α of 300 W/m^2/K.
- Hold for 12 hours at 1550 °C with a heat transfer coefficient α of 300 W/m^2/K.
- Adiabatic conditions are assumed for the top and bottom surfaces of the pilot steel ladle.

The insulation bricks vertically support the pilot ladle at the bottom surface. Therefore, in the numerical models, the pilot ladle is supported vertically (with no tensile stiffness), and for in-plane sliding, a friction coefficient of 0.5 is assumed. The self-weight of the materials is considered in the analysis.

For the mortarless masonry in the working lining, a dry joint of 0.2 mm is assumed for the bed and head joints. For the shear behaviour of these joints, temperature-dependent values of friction coefficient are used (Table 4). For the interaction between the working lining and permanent lining, a gap of 0.2 mm with a friction coefficient of 0.5 is assumed. A similar interaction is considered for the permanent lining and insulation board interface. For the interface behaviour between insulation board and steel shell, a rigid normal behaviour with a friction coefficient of 0.5 is assumed.

Table 4 - Friction coefficient values for dry joints at different temperatures [5].

Temperature (ºC)	20	300	600	900
Friction coefficient (-)	0.598	0.498	0.510	0.530

The following sections present the results obtained with numerical simulations considering different modelling approaches. The geometry, material properties, thermal loads and boundary conditions used in the models are identical, as presented in this section.

3 Micro-modelling approach

In this approach, the spatial discretisation of the masonry is performed at the level of brick elements, and the dry joints are represented by their contact behaviour using interface elements. Herein, brick elements are simulated with corresponding mechanical parameters of the material from which they are made and their connection with contact elements that permit separation, penetration and sliding at the contact (further details of the normal behaviour of the dry joint is presented in Deliverable 2.6). Additional information regarding this approach is presented in Deliverable 3.6.

A 3D partial ring model of a pilot steel ladle (Figure 5a) is made in Abaqus software [12] taking advantage of the periodic thermal and mechanical boundary conditions of the structure. The working lining was modelled as a mortarless masonry (i.e., individual brick units and dry joints as interfaces), as the primary focus of this simulation is to evaluate the behaviour of the working lining. Different thickness of the working lining observed in the Figure 5b showing the cross-section is due to the cylindrical arrangement and section cut chosen. Masonry present in the permanent lining is modelled as an equivalent homogenous material. All the linings are meshed with 3D hexahedron elements (C3D8T) of approximately 7×7×7 mm^3 size. This model consists of 197900 material elements and 142944 interface elements. In the model, elastic-viscoplastic behaviour is considered only for the bricks in the working linings. The rest of the model is deemed to be elastic. The material properties, thermal load and boundary conditions are the same as presented in the previous section. Coupled thermal-displacement analysis was carried out for this simulation in which the pilot ladle was first subjected to gravity load, thermal heating and then temperature hold.

European Commission | Horizon 2020 European Union funding for Research & Innovation

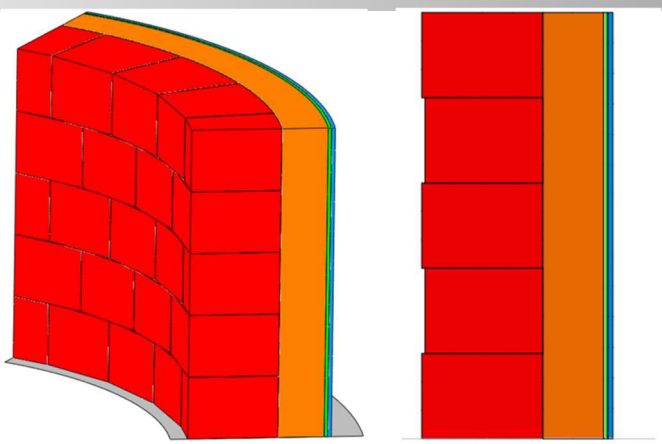

(a) (b)

Figure 5 - Full-scale micro-model of pilot steel ladle:
a) global view presenting different linings and a rigid base; b) cross-section of the FE model.

3.1 Thermal behaviour

Figure 6 shows the temperature distribution over the pilot ladle at the end of the analysis (i.e., 24.75 hours). Temperature distribution along the vertical direction is identical for all the linings (Figure 6). This distribution is expected due to the assumed thermal boundary conditions. The surface temperature at the hot face of the working lining is around 1510 °C, and it reduces to 280 °C at the cold face of the steel shell. Temperature distribution along the linings is presented in Figure 7. The distance is shown from the hot face of the working linings. The temperature at the hot face of the working lining is 1510 °C, and it reduces to 830 °C at the interface between the working and permanent lining. The temperature further reduces to 530 °C at the interface between the permanent lining and the insulation board, where it reduces to 283 °C at the steel shell. The effectiveness of the different refractory layers to prevent heat loss can be observed in the figure. This temperature distribution is similar to the distribution in an industrial steel ladle due to a similar configuration of layer thickness.

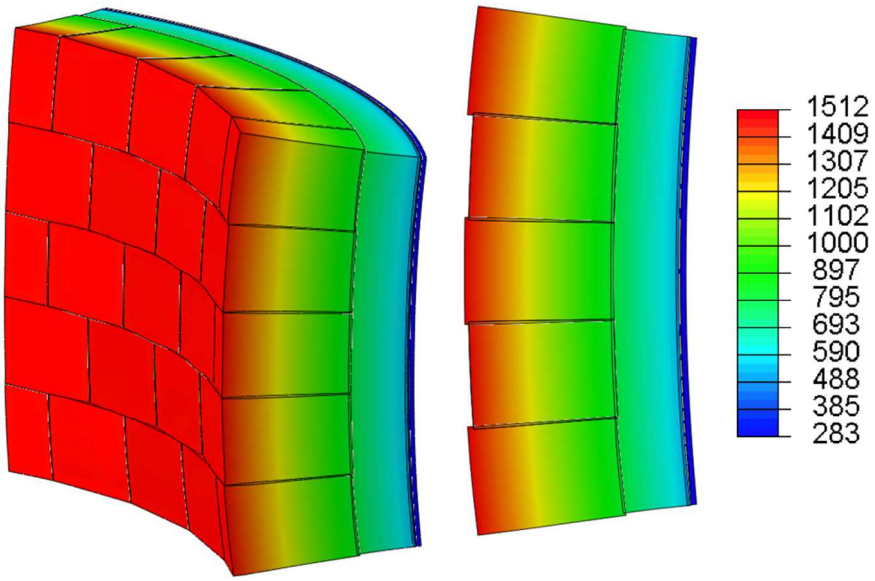

(a) (b)

Figure 6 - Temperature distribution in the pilot steel ladle at the end of analysis (24.75 hours) with deformations magnified by 15 times: a) global view; b) cross-section. Legend shown is in °C.

European Commission | Horizon 2020 European Union funding for Research & Innovation

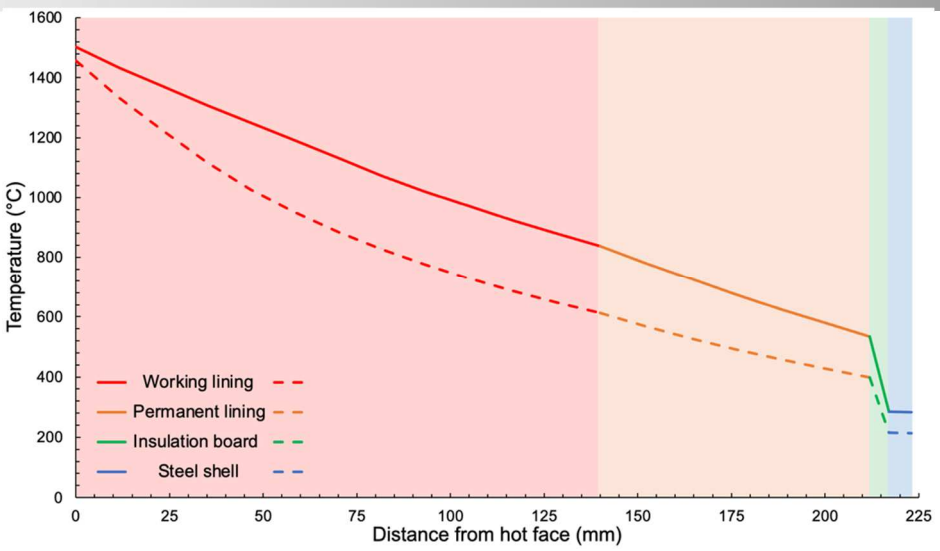

Figure 7 - Temperature distribution in the different linings of the pilot steel ladle, from the hot face of the working lining to the cold face of the steel shell. Solid line represents distribution at the end of the experiment (24.75 hours) and dotted line at the end of heating (12.75 hours).

Figure 8a presents the evolution of temperature at different locations in the linings of the pilot ladle. The temperature evolution is shown for the hot face of the working lining, for the cold face of the working lining, for the cold face of the permanent lining, and at the cold face of the steel shell (Figure 8b). The input furnace temperature is shown as a reference. The rise in temperature in different linings is expected due to given thermal loading and boundary conditions. A steady rise in the hot face temperature can be observed during the heating period, which is similar to the input furnace temperature. A slight increase in temperature can be observed during the hold period for the hot face. For the whole duration of the simulation, a temperature rise can thus be observed in the different linings of the pilot ladle. This temperature evolution with time is similar to the change observed from the in-situ measurements of an industrial steel ladle (Deliverable 4.4).

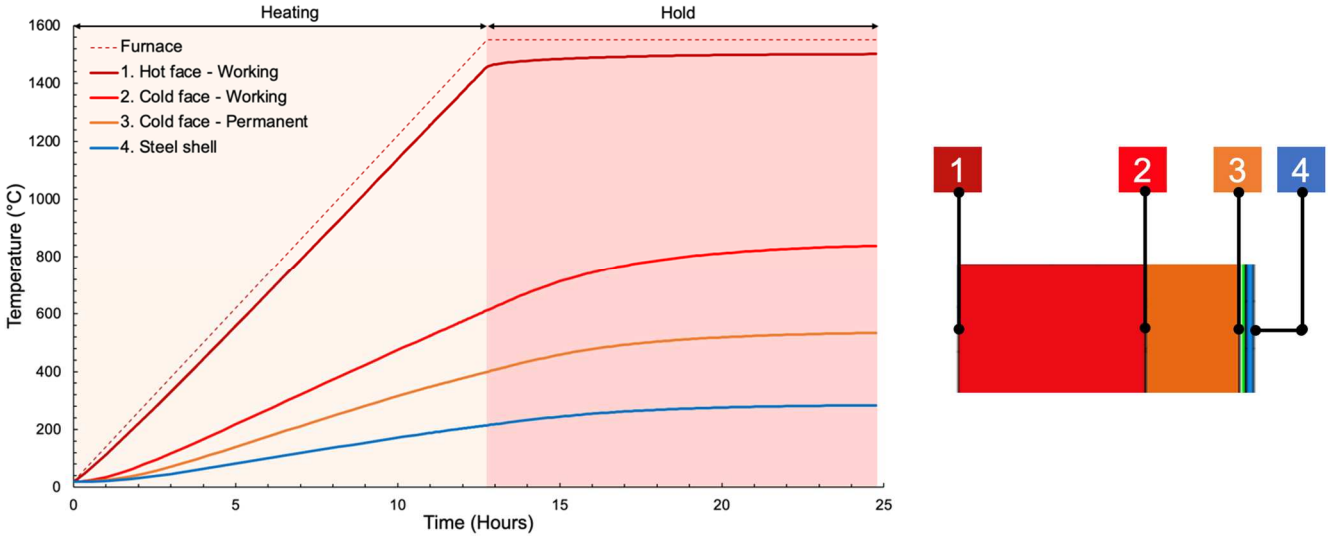

(a) (b)

Figure 8 - Evolution of temperature with time: a) distribution in the different linings of the pilot steel ladle; b) location of the obtained temperature evolution in the linings.

3.2 Mechanical behaviour

Global and local (joints between bricks and other layers) mechanical boundary conditions along with temperature gradient in the linings generate strains and stresses in the materials. This effect leads to local and global deformation of the pilot ladle. The evolution of stresses and strains in the working lining (considering elastic-viscoplastic properties) are discussed in this section.

Radial behaviour indicates the performance of the linings in the radial direction (considering the cylindrical coordinate system) for the pilot steel ladle. The temperature gradient primarily influences the behaviour in this direction along with the thickness of the linings and the behaviour of the interface between different linings. Circumferential behaviour is mainly controlled by the dry joint

European Commission | Horizon 2020 European Union funding for Research & Innovation

in the head joint and thermal elongation. The behaviour of the working lining in the vertical direction is influenced by the gravity load, dry joint in the bed joint and thermal elongation. The evolution of these stresses at the hot face of the centre of the working lining from the 3rd layer (i.e., 250 mm height from the base) is presented in Figure 9. From the figure, it can be noticed that the level of stress in the circumferential direction is larger compared to the other directions. This difference is due to the global and local mechanical boundary conditions. The pilot ladle is only supported at the bottom in the vertical direction, and the expansion in that direction is only restricted by the self-weight of the working lining bricks.

Similarly, in the radial direction, due to the thermal expansion of the other linings, the expansion of the working lining is not significantly restricted. For the circumferential direction, closing of dry joints at the hot face can be observed at the 3rd hour of the heating period, subsequently, another change can be observed between 7th and 11th hour. This change is due to the progressive reduction of the stiffness of working lining bricks at higher temperatures. After 11 hours a sudden drop in the circumferential stress is observed once the surface temperature of the hot face reaches the set value of creep initiation at 1300 °C.

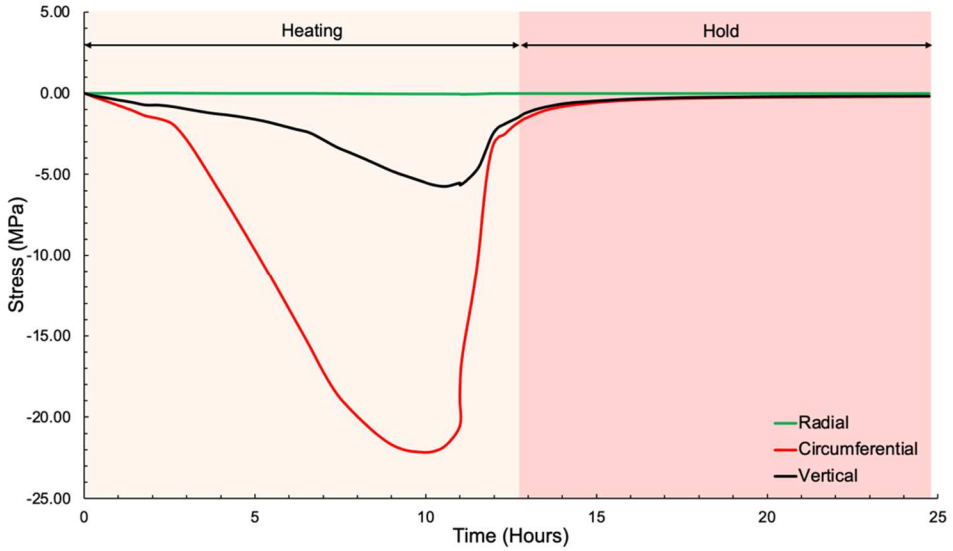

Figure 9 - Evolution of the stresses in the centre of the working lining (hot face) from a brick in the 3rd layer.

Once the hot face experiences change in material stiffness and relaxation, progressive transfer of stresses follows within the thickness of the working lining, as shown in Figure 10. Moreover, Figure 10 shows that the circumferential stress at the centre of the working lining thickness (i.e., 70 mm from the hot face) does not go under relaxation. This is due to the temperature at that point, which is lower than the creep initiation temperature of 1300 °C.

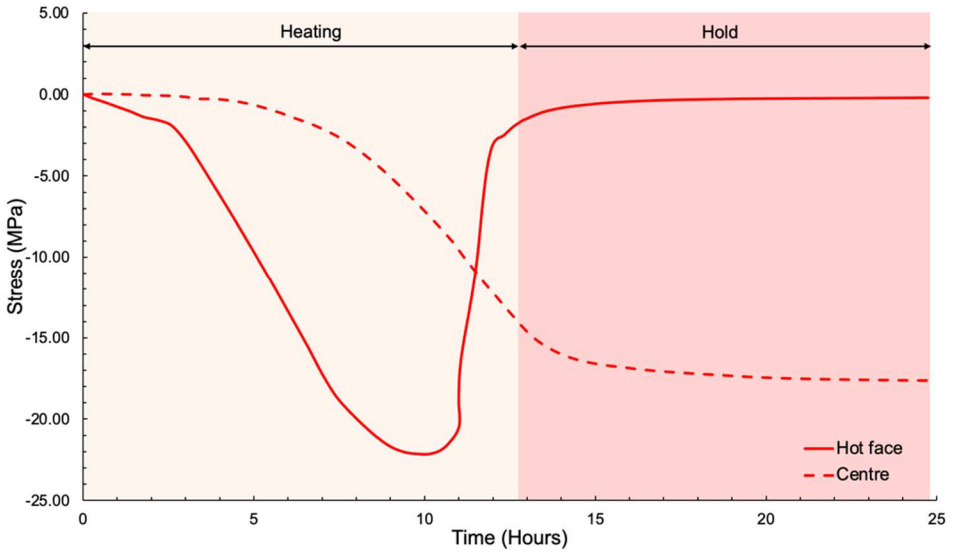

Figure 10 - Evolution of the circumferential stresses at the hot face and centre (70 mm from hot face) of a brick in the 3rd layer of the working lining.

Figure 11 presents the evolution of different strains in the circumferential direction at the hot face of the working lining at 250 mm height from the base. Total strain observed in the hot face is composed of elastic strain, thermal strain and creep strain. From the figure, it can be noticed that a significant part of the strain observed is due to thermal strain. This is expected due to high-

European Commission | Horizon 2020 European Union funding for Research & Innovation

temperature exposure. Once the temperature starts to increase from the ambient temperature, thermal strain increases. Concurrently, the elastic strain stays at zero due to the closure of the head joints. Once the joint is closed, the compressive elastic strain increases. When the creep initiation temperature is reached, a sudden increase in creep strain and a decrease in elastic strain is observed.

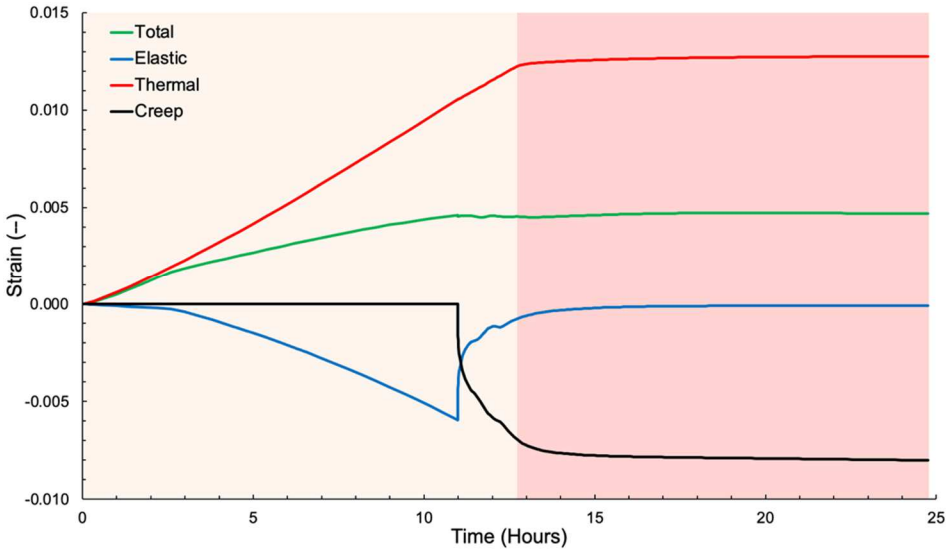

Figure 11 - Evolution of the strain in the centre of the working lining hot face from a brick in the 3rd layer.

The distribution of the circumferential stress and creep strain at the end of the analysis is shown in Figure 12. A low level of stress can be noticed near the hot face of the working lining due to the high amount of creep. At the centre of the working lining, a concentration of high stress can be observed; this is due to the presence of less creep, which forces the concentration of the stress. Figure 12b shows zero creep strains from the centre of the working lining. This is due to the distribution of temperature levels that are below the creep initiation.

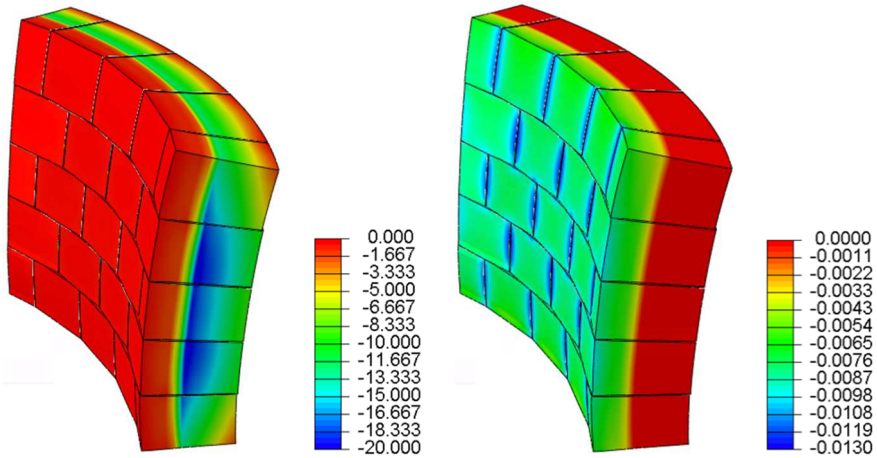

Figure 12 - Behaviour of the working lining of the pilot steel ladle: a) Distribution of the circumferential stress (MPa); b) Distribution of the creep strain in the circumferential direction (-).

4 Macro-modelling approach

Using Abaqus finite element software, the numerical model of the pilot ladle was developed. The macro-FE model of the pilot is shown in Figure 13. Due to the symmetry of the pilot ladle, only one quarter was considered. The two insulation layers laid on top of the steel support of the test setup have been modelled as a rigid plate. The working lining (bricks and joints) were replaced by a homogeneous material whose mechanical properties depend on the state of bed and head joints (open or closed). Further details about the development and validation of the homogeneous material model of masonry with dry joints are given in deliverables 3.6 and 3.8.

European Commission | Horizon 2020 European Union funding for Research & Innovation

The modelling strategy was as follows: first transient heat transfer analysis was carried out to determine the temperature distributions of the different layers. Then, transient thermomechanical analysis was performed to determine the stress and strain fields. The thermal boundary conditions of the heat transfer analysis are similar to those reported in the micro modelling technique. The thermophysical and mechanical properties of the different layers are given in section 2.

The frictional interactions between the contact surfaces of the different layers and the rigid plate were considered with a coefficient of friction of 0.5. In addition, the frictional interactions between the working, safety, insulation layers and steel shell were considered with a value of friction coefficient equal to 0.5. The rigid plate was considered as fully fixed. Symmetry boundary conditions were applied to the symmetric planes of the solution domain. The gravity effects are considered in the numerical model.

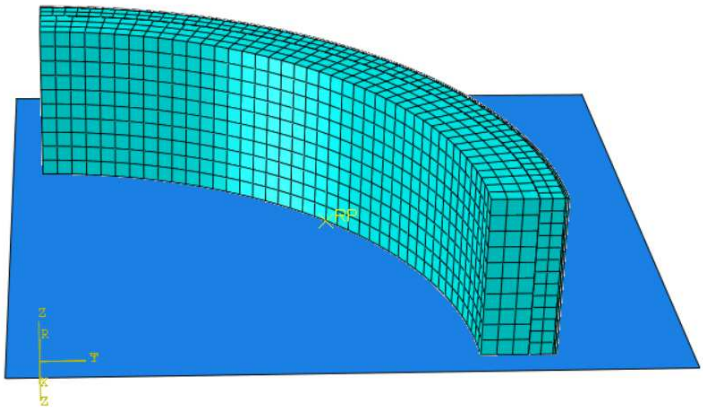

Figure 13: Physical model of the macro modelling approach.

The temperature results are shown in Figure 14. The temperature variations of the working lining HF and CF as well as the temperature variations of the safety lining cold face and steel shell are shown in Figure 15a. The temperature field at the end of the holding step is given in Figure 15b. The temperature gradient through the different layers at the end of the heating and holding steps are given in Figure 15c. At the end of the holding stage (i.e. steady state), the temperature at the hot face of the working lining is around 1500 °C, and it reduces to around 800 °C at the interface between the working and permanent lining. The temperature further reduces to about 500 °C at the interface between the permanent lining and the insulation board, where it decreases to 280 °C at the steel shell.

European Commission | Horizon 2020 European Union funding for Research & Innovation

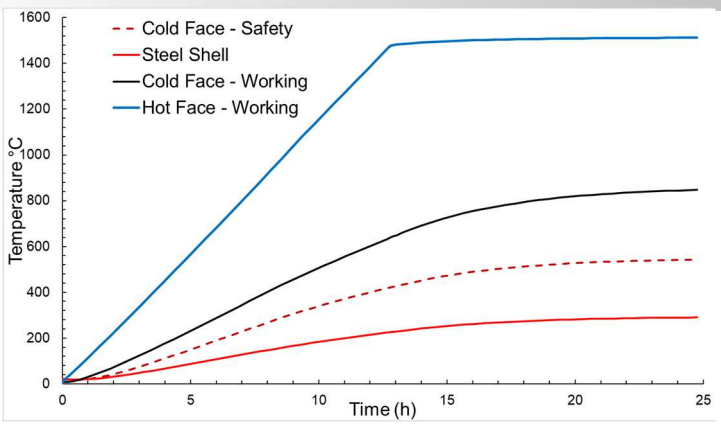

(a)

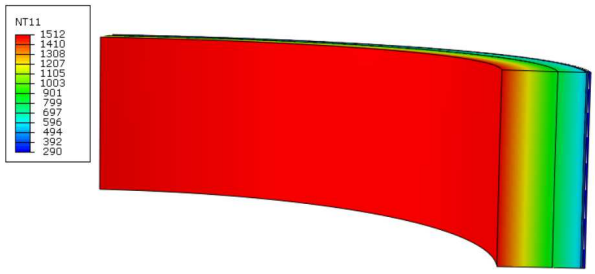

(b)

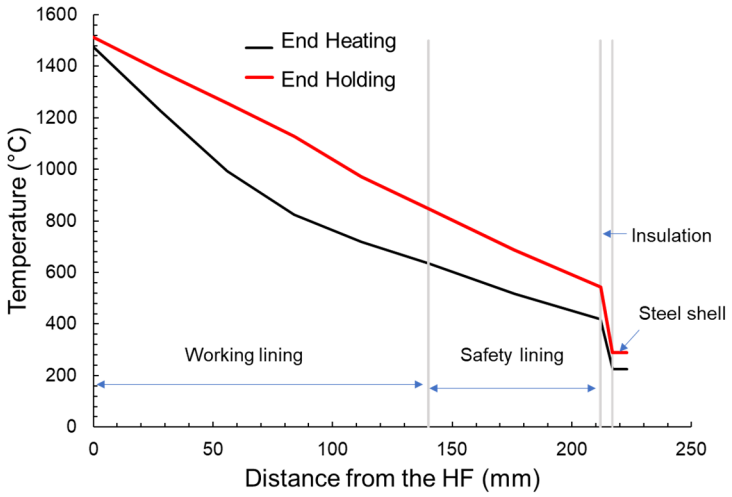

(c)

Figure 14: Results of the heat transfer analysis: (a) Temperature variations of the different layers of the lining with time obtained from the macro model. (b) Temperature fields at time = 24.75 h (end of the simulation time, given in °C). (c) Temperature gradients through the thickness of the different layers at the end of the heating and holding stages.

Time evolutions of the thermal stresses (in the radial, circumference and axial directions) in the hot face of the wall (middle, H = 250 mm) of the working lining during the heating and holding steps are shown in Figure 15a. In general, it has been observed that, in the first nine hours, the resulting compressive thermal stresses increased gradually with the increase of the temperature. Next, the stresses decreased sharply (when the temperature of the hot face reached the set value of creep starting temperature 1300 °C) to around -2 MPa due to stress relaxation. This decrease in stresses in the hot face was, on the other hand, equivalent to an increase in the stresses in the middle of the brick (see Figure 15b). It can also be observed that the stresses in the radial and axial directions are very small. This is mainly caused by the free expansion of the working lining in the axial direction as shown in Figure 16.

European Commission | Horizon 2020 European Union funding for Research & Innovation

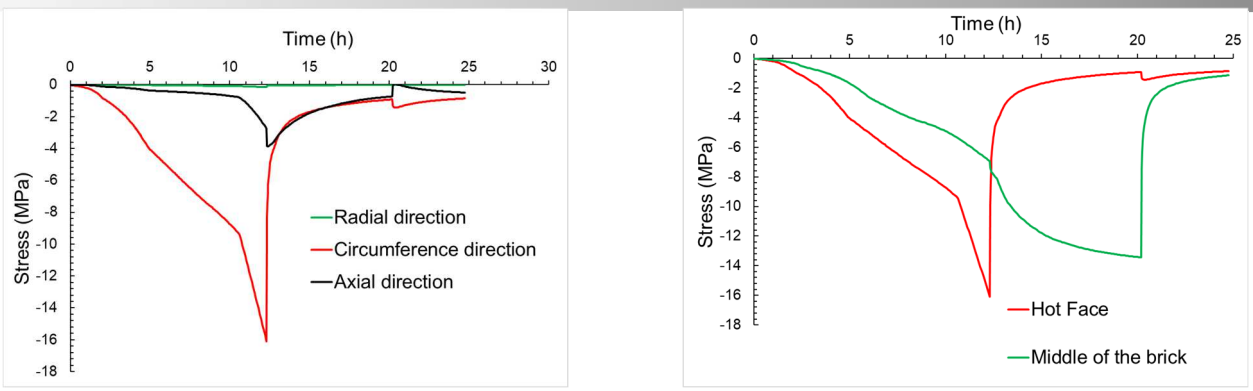

(a) (b)

Figure 15: Thermomechanical analysis: (a) Variations of the stresses vs. time in the hot face of the working lining and (b) comparison between the circumference stresses in the hot face and middle of the brick.

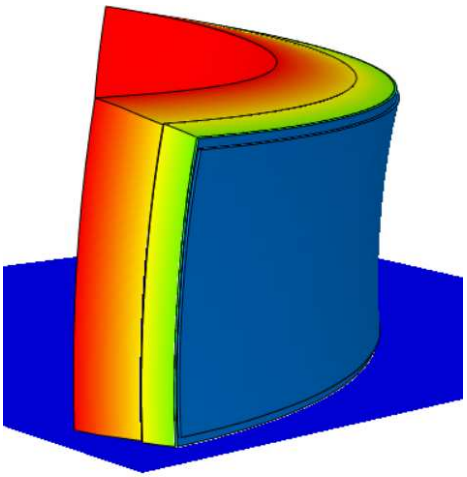

Figure 16: Deformed shape of the pilot ladle showing the difference in thermal expansion of the different layers due to temperature gradient.

The in-plane viscoplastic strains in the wall (in θθ direction) of the working lining of the steel ladle by the end of the simulation is given in Figure 17. It can be seen that the highest values of viscoplastic strains are located near the HF of the wall in the θθ direction due to its higher temperature. The viscoplastic strains in the CF of the wall is almost zero. This can be attributed to the calculated temperatures of the CF of the wall (presented in Figure 15) always being below the set value of creep initiation temperature (1300 °C).

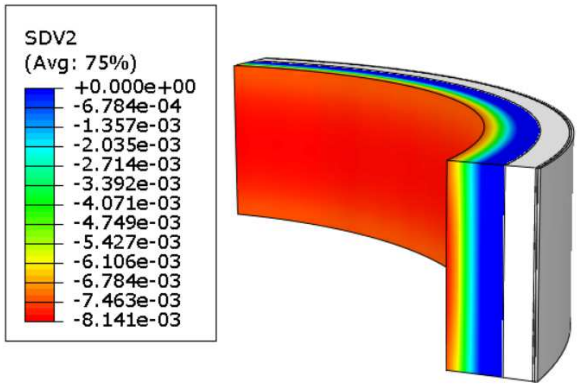

Figure 17: Viscoplastic strains in the working lining by the end of the holding stage.

European Commission | Horizon 2020 European Union funding for Research & Innovation

5 Conclusion

The 3D pilot ladle, a novel experimental installation developed within ATHOR, represents a unique approach toward large-scale refractory masonry. The experimental campaign will provide a large set of measurement data under a pure thermal load application (i.e., without corrosion effect due to molten steel). This characterisation will ultimately provide insights into the thermomechanical behaviour of refractories in a cylindrical shape, such as joint behaviour, the interaction between the linings, creep, plasticity, and material damage.

The present document describes the predictive response of the pilot steel ladle with numerical simulations. The document presents numerical results using different modelling approaches employed within the ATHOR project, micro-model, and macro-model. Both models predict a significantly high concentration of the stresses in the circumferential direction. The evolution of the stress and creep strain in the working lining is shown for both modelling approaches. The obtained results are in a similar range and describe a similar response.

These results will be used to calibrate advanced nonlinear micro and macro numerical models once the experimental data are available. This calibration process will give essential data regarding the influence of different material and geometric parameters on the global behaviour of the pilot ladle. Identifying these critical parameters will validate the numerical models with the industrial steel ladle and assist in optimising the material utilisation of different refractory linings using these modelling approaches.

6 References

[1] Schacht, C. A., *Refractory lining: Thermomechanical design and applications. Mechanical Engineering*. 1995.

[2] Jin, S., H. Harmuth, and D. Gruber, “Compressive creep testing of refractories at elevated loads—Device, material law and evaluation techniques,” *Journal of the European Ceramic Society*, vol. 34, no. 15, pp. 4037–4042, Dec. 2014, doi: 10.1016/J.JEURCERAMSOC.2014.05.034.

[3] Breder Teixeira, L. *et al.*, “Experimental Investigation of the Tension and Compression Creep Behavior of Alumina-Spinel Refractories at High Temperatures,” *Ceramics*, vol. 3, 2020, doi: 10.3390/ceramics3030033.

[4] Andreev, K., S. Sinnema, A. Rekik, S. Allaoui, E. Blond, and A. Gasser, “Compressive behaviour of dry joints in refractory ceramic masonry,” *Construction and Building Materials*, vol. 34, pp. 402–408, Sep. 2012, doi: 10.1016/J.CONBUILDMAT.2012.02.024.

[5] Oliveira, R. L. G., J. P. C. Rodrigues, J. M. Pereira, P. B. Lourenço, and H. Ulrich Marschall, “Normal and tangential behaviour of dry joints in refractory masonry,” *Engineering Structures*, vol. 243, p. 112600, 2021, doi: 10.1016/j.engstruct.2021.112600.

[6] Oliveira, R. L. G., J. P. C. Rodrigues, J. M. Pereira, P. B. Lourenço, and H. U. Marschall, “Thermomechanical behaviour of refractory dry-stacked masonry walls under uniaxial compression,” *Engineering Structures*, vol. 240, no. December 2020, 2021, doi: 10.1016/j.engstruct.2021.112361.

[7] Prietl, T., “Ermittlung materialspezifischer Kennwerte von feuerfesten Werkstoffen und Zustellungen unter uni- und biaxialen Lastbedingungen für die Nichteisenmetallindustrie,” 2006.

[8] Oliveira, R., J. P. Rodrigues, J. Pereira, P. Lourenco, and R. Lopes, “Experimental and numerical analysis on the structural fire behaviour of three-cell hollowed concrete masonry walls,” *Engineering Structures*, vol. 228, p. 111439, 2021, doi: 10.1016/j.engstruct.2020.111439.

[9] Samadi, S., S. Jin, D. Gruber, H. Harmuth, and S. Schachner, “Statistical study of compressive creep parameters of an alumina spinel refractory,” *Ceramics International*, vol. 46, no. 10, pp. 14662–14668, 2020, doi: 10.1016/j.ceramint.2020.02.267.

[10] Vitiello, D., “Thermo-physical properties of insulating refractory materials,” Ph.D thesis, Université de Limoges, 2021.

[11] Kaczmarek, R., “Mechanical characterisation of refractory materials,” Ph.D thesis, Université de Limoges, 2021.

[12] Smith, M., *ABAQUS/Standard User’s Manual, Version 2019*. United States: Dassault Systèmes Simulia Corp, 2019.

European Commission | Horizon 2020 European Union funding for Research & Innovation